Refrigeration performance and the elastocaloric effect in natural and synthetic rubbers

R. Bennacer, B. Liu, M. Yang, A. Chen

Refrigeration performance and the elastocaloric effect in natural and synthetic rubbers

R. Bennacer[1,2*], B. Liu[1], M. Yang[1], A. Chen[1]

[1]Tianjin Key Lab of Refrigeration Technology, Tianjin University of Commerce, P.R.C., 300134.

[2] Université Paris-Saclay, ENS Paris-Saclay, CNRS, LMT, Laboratoire de Mécanique et Technologie, Gif-sur-Yvette, France

*Corresponding author: rachid.bennacer@ens-paris-saclay.fr

Abstract: Elastocaloric cooling, also known as thermoelastic cooling, has been identified as a promising alternative to current state-of-the-art vapour compression cooling systems which tend to use environmentally unfriendly refrigerants. In this study, five different types of rubbers including natural rubber, silicone rubber, cis-butadiene rubber, styrene-butadiene rubber and chlorosulfonated polyethylene were investigated as working materials for thermoelastic cooling applications. A setup and protocol was developed to investigate and quantify the cooling effect of the rubbers during stretching and releasing cycles. The results show that for all five rubbers, the mechanical response of the stress–strain curve depends on the maximum loading. This is previously studied and named as Mullins effect. Such effect was negated after nine cycles of loading andunloading. The Coefficient Of Performance (COP) for the studied materials were quantified to compared to the performance of the investigated working materials. The natural rubber was found to be the working material with the best performance worth further exploration with a COP of more than 2. The cycle analysis of this material shows that the temperature difference of such system is around 7K which shows a great potential for applications in cooling systems.

Key words: Elastocaloric effect, Refrigeration, Coefficient Of Performance , Mullins effect

1 Introduction

Refrigeration plays an important role in a wide range of industrial activities. This application tends to use substantial amounts of energy. Environmental and efficiency constraints led to research activity exploring new concepts for refrigeration. Researchers are therefore very keen on developing alternatives to the relatively inefficient (about 20% efficiency with respect to power input) vapour compression systems which are widely used today. Vapour compression refrigeration cycle are worth replacing because they tend to be noisy and use fluids which have detrimental environmental impact [1].

In recent decades, several alternatives to vapour compression cycles were proposed and developed [2]. Unfortunately, either because of low efficiency and low specific power or impracticality, none of these concepts has proven to be a serious alternative for cooling needs. However, more recently the so-called caloric cooling technologies have shown great potential as serious alternatives to vapour compression technology [2]. By caloric cooling technologies, it is meant magnetocaloric (magnetic), electrocaloric, elastocaloric and barocaloric cooling. The basis of caloric cooling is to exploit the latent heat of a solid-state phase transformation of a ferroic material by applying an external magnetic, electric or mechanical field [3]. These technologies can be significantly more efficient (with theoretical exergy efficiency above 50 %), completely harmless to the environment (by applying solid-state refrigerants) and potentially, vibration and noise free [4]. Amongst the caloric cooling technologies, the most advanced and developed is the magnetic (magnetocaloric) refrigeration with up to 100 prototypes developed in universities and laboratories around the world [4] and [5]. However, more than 20 years of research on magnetocaloric materials and magnetic refrigeration systems is still unsuccessful in providing the necessary breakthrough that could lead to a commercial realisation of this technology and satisfy the urgent global need for a more efficient and environmentally friendly refrigeration. The possibility of inducing a solid-state phase transformation via phase transformation and generating a caloric effect by means of mechanical stress *i.e.* the elastocaloric effect (**eCE**) in superelastic shape-memory alloys (**SMAs**), opens new avenues for solid-state refrigeration.

The elastocaloric effect, involves compressing and decompressing single crystalline (or polycrystalline) materials. Elastocaloric materials are attractive because they tend to have larger

reversible temperature changes than magnetocalorics. They also tend to be less expensive, comprising alloys of metals rather than more pricy rare-earth magnets [6].

The elastocaloric effect occurs when a material undergoes a transition in its crystal structure when it is compressed [7], *i.e.* change in conformational entropy (lower entropy of long polymeric chains stretches). A material must undergo a large change in volume during the structural phase transition and the material must have mechanical properties that are compatible with being repeatedly compressed amd decompressed. Furthermore, the material should be polycrystalline so that it can be easily and cheaply manufactured in bulk. Ni-Ti alloy is the most widely used Shape-Memory Alloy (SMAs) and occupies a dominant position in the market, it can achieve a temperature rise of 20K with applied stress of approximately 200 MPa above the stress level associated with the end of the transformation plateau. However, its two-step transformation and asymmetric transformation path [8,9] indicate that it has a higher transformation hysteresis, which results in its fatigue lifetime as a refrigerant running far less than 10 years, equivalent to 78 million stress-induced transformations (cycle of ¼ Hz).

Adding copper to Ni-Ti alloy can effectively improve its fatigue lifetime [10,11]. This is because the addition of copper not only changes the transformation path, but also improves the crystal compatibility between the parent phase and the child phase, thus reducing the hysteresis phenomenon and improving fatigue characteristics [12,13]. The fatigue limit of Ti rich $Ti_{54}Ni_{34}Cu_{12}$ alloy increased to 10^7 cycles without any degradation of the effect. The ternary alloy in the copper-based alloys improves the mechanical and thermal properties of the binary alloy, while the Cu-Al-Ni and Cu-Zn-Al alloys in the ternary alloy are the most promising copper-based materials with high latent heat [14]. However, all copper-based materials face the same fatal problem, that is, their brittleness limits their application in elastocaloric refrigeration [15]. Although iron-based materials have no brittleness similar to copper-based materials, their latent heat of transformation is far less than that of nickel-based and copper-based alloys, which can be improved by adding other elements [16]. Li et al. used the concept of high entropy alloy to develop a high entropy alloy (Polycrystalline $NiCuTiHf_{0.6}Zr_{0.4}$) with a wide temperature range hyperelasticity and huge **eCE** [17]. The alloy exhibits perfect hyperelasticity with fully recoverable strain in the temperature range of 263~463k，the maximum adiabatic temperature difference is 9.3K. Yoshida et al. found that poly (vinylidene fluoride trifluoroethylene chlorotrifluoroethylene) [P (VDF TrFE CTFE)] terpolymer has strong **eCE**, when the strain is 12%. The reversible adiabatic temperature difference is 2.15K [18].

However, compared with Ni-Ti alloy and PVDF-based polymers, rubber has lower tensile stress, lower cost, larger cooling capacity and relative larger volume (at the same mass), fatigue resistance and fatigue damage can be addressed at high temperature, which has great potential in the field of elastocaloric refrigeration [19].

Although thermodynamic studies of rubber elastomers can be traced back to 1859 (Gough-Joule effect) [20], few people have so far put it into practice. Dart et al. [21] explored the influence of rapid stretching on the temperature rise of natural rubber and synthetic rubber in 1942. Daniel et al. [22] obtained the overall description of the temperature differential equation of materials under mechanical stress through a theoretical analysis. Xie et al. [23,24] studied the **eCE** of natural rubber after pretension, the direct measurement and indirect measurement of the **eCE** of natural rubber are compared. Wiegand [25] proposed two designs of elastomer cycle, Hayward [26] proposed a swing cylinder engine, and Gerlach et al. [27] built a concept prototype. Xie et al. [28] obtainedthe **eCE** of natural can be produced in the temperature range of 273-322K, and the maximum adiabatic temperature difference is 12K at 283K. Wang et al. [29] twisted rubber fibers, untwisting and stretching the twisted rubber fibers at the same time, which produced higher refrigeration effect.

To the best of our knowledge, very few studies are devoted to test the energy performance of elastocaloric materials in a complete investigation in a caloric refrigeration system. Aprea et al. [30, 31] tested the benchmark NiTi and the CuZnAl both for cooling [30] and a heat pump [31] applications and found for example that mechano-caloric materials have the most sensible heat effect in heat pump applications. This is due to the heating capacities achieved at acceptable costs. Apart from these investigations which are part of wider studies devoted to comparing the performance of different caloric materials, in literature there is no analysis devoted to elastocaloric material..

This paper explores five selected rubber materials to study the Mullins effect and the thermal performance after use(elimination of Mullins effect). Results from the experimental investigation combined with the thermodynamic properties of rubbers enabled the selection of the best material.

2. Experimental Procedures

2.1 Materials and experimental setup

For the purpose of this investigation, the selected materials are natural rubber, silicone rubber, cis-butadiene rubber, styrene-butadiene rubber and chlorosulfonated polyethylene. These were produced by Vanke polymer new material technology Co., Ltd. The structure, shape and size of the samples used is shown in Figure 1, the thickness of the material is 2mm and the relevant physical properties of the

materials are shown in Table 1.

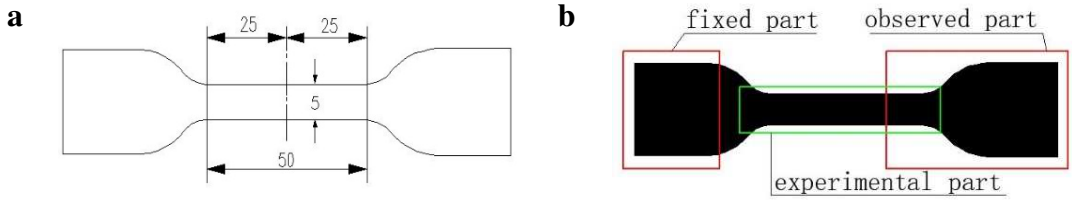

Fig. 1 Experimental sample. **a**. Sample dimensions (in mm). **b.** Different parts of the sample in the experiment.

Table 1 Properties of rubber (from [2, 5, 7])

Rubber type	Density [gcm^{-3}]	Specific heat capacity [$J(kg\cdot K)^{-1}$]	Thermal conductivity [$W(m\cdot K)^{-1}$]	Operating temperature range [30] [K]	Shore A hardness	Mooney viscosity $ML_{1+4}^{100℃}$
Natural rubber	1.11	1341	0.267	198~363	53	62
Silicone rubber	1.17	1278	0.253	153~553	60	45
Cis-butadiene rubber	1.18	1269	0.371	-100~100	67	55
Styrene-butadiene rubber	1.20	1265	0.428	213~373	69	62
Chlorosulfonated polyethylene	1.40	1110	0.529	213~423	71	49

The specific heat capacity of rubber is calculated using the following formula:

$$c_p = \frac{e^2}{\lambda\rho} \tag{1}$$

Where the thermal conductivity λ (W $(mK)^{-1}$) and the thermal effusivity, e ($Ws^{1/2}m^{-2}K^{-1}$) were measured by a thermal conductivity analyzer C-Therm TCi.

2.2. Experimental setup

The experimental setup is composed of two parts. One is a FLS40 series screw linear module (Chengdu Fuyu Technology Co., Ltd.), which is equipped with a controller, a driver and a DC power supply. The controller allows less than 1% error on the maximum used value in the present study. The other is a home-built fixture which is fixed on the module, it is mainly made of an aluminum plate and tightened with nuts to fix the rubber, as shown in Figure 2. The infrared thermal imager is used for temperature measurement (FLIR X6520sc). It is fixed at a distance of 72cm from the rubber, the recording speed is 30fps and the reflectivity of natural rubber is considered of 0.95.

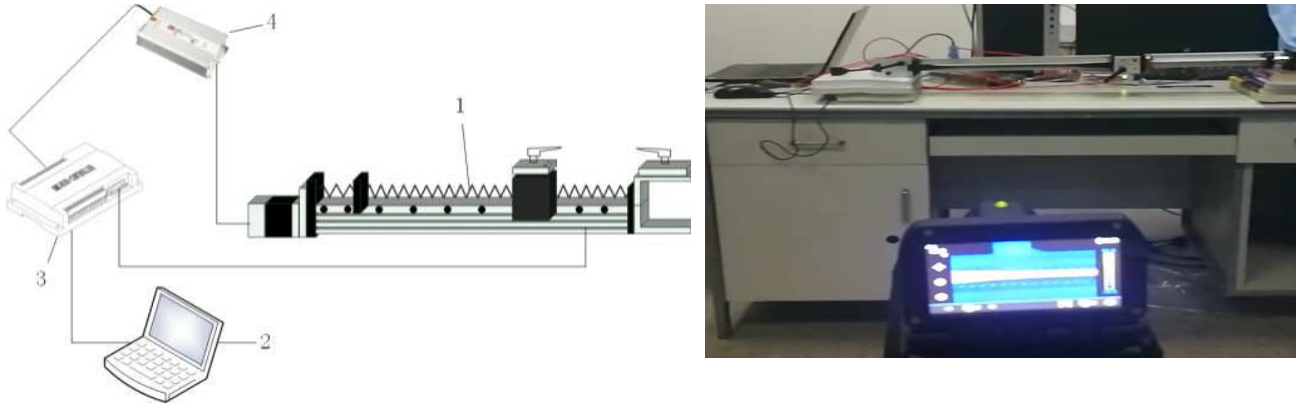

(a) (b)

Fig. 2 Experimental setup. **a.** Experimental diagram. (1) FLS40 series screw linear module; (2) driver; (3) controller; (4) DC power supply. **b.** Overview of the experimental setup

2.3. Methods

The experimental procedure consists of fixing the two ends of the rubber sample to the fixture, then set the stretching speed (elongation rate) and stretching displacement on the controller. Once the stretching stage is finished, we record the temperature of the observed part with the infrared thermal imager. The obtained stress (induced force at the end of stretching stage, i.e. inner stress $\sigma<0$) will be maintained at a relatively constant value in order to follow the right cycle. When the rubber sample cools to ambient temperature, we drive the rubber sample to return to the initial state following the same speed. After the release of the sample (constant zero stress, $\sigma=0$), the temperature of the observed part is recorded. When the rubber sample reaches the ambient temperature, we carry on the stretching stage of the rubber to complete the next cycle. The cycle consists of four stages: stretching stage, cooling stage, recovery stage and heating stage. The cycle diagram and temperature entropy diagram are shown in Figure 3. The heat pump cycle ability is described by the work (W) and the energy, Qc from cold reservoir to hot reservoir, Qh. The sink and source allow the generation of a cooled sub-domain (equivalent to the ambiant close to the evaporator and condenser in a conventional system) and the potential is given by an induced temperature difference during stretching and return to the initial position. In the present protocol we also aim to identify the heat transfer characteristic time (between elastomer and the ambient environment) so we will use this to extrapolate from a thermodynamic cycle (energy: green dashed area on figure 3 illustrating the cooling/heating from hot temperature to ambient) to potential power.

In order to study the influence of different elongations and elongation rate on rubber temperature change, we set the (elongation rate) as being 50, 200 , 600 $mm.s^{-1}$ and 200, 400 and 600% of the tensile length, respectively.

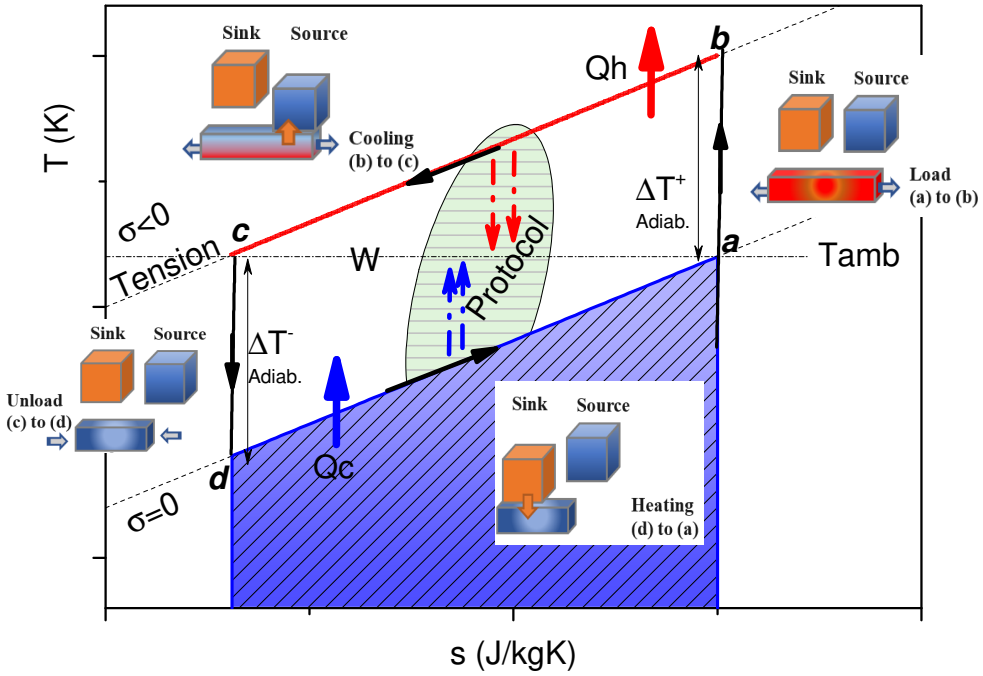

Fig. 3 Characterization protocol within the Elastocaloric refrigeration cycle diagram and temperature entropy diagram.

3 Tests of rubber materials

In Elastocaloric processes, Mullins effect is an important factor. Mullins effect [33] is a phenomenon of initial softening of stress-strain curve. As a type of elastocaloric material in solid-state refrigeration, rubber must eliminate this Mullins effect before it can be used in the process. Therefore, all the experimental studies conducted in this study are based on this concept, that is to say, the experimental samples after training (eliminate Mullins effect) are used. In these experiments, the tension recovery-cycle experiments were carried out on the electronic universal testing machine (AG-IC 50KN, Shimadzu Mangt. China Co., Ltd.), the measurement accuracy is ±0.5%, and the temperature measurement is carried out by an infrared thermal imager (FLIR X6520sc). The five types of rubber test strips were loaded with a cyclic elongation rate of 500mm. min^{-1}, the maximum elongation of the rubbers; natural, silicone, cis-butadiene rubber, styrene-butadiene and chlorosulfonated polyethylene were 400mm (800%), 400mm (800%), 250mm (500%), 300mm (600%) and 150mm (300%) respectively.

The stretching-releasing cycle is repeated 9 times. The recorded corresponding Stress-Strain (elongation) are given in figure 4-a for natural rubber. Reversibility of the cycle is observed after 6 cycles. The achieved reversibility (training) matches to the suppression of the Mullins effect. Similar

behavior is observed for the different working materials.

The Stress- elongation reversible cycle for the different materials are presented in figure 4-b. Note that different materials exhibit different maximum elongation. This is due to the maximum sustainable elongation because of the mechanical properties of the material. Nevertheless, the maximum stress is found not to be correlated to the elongation. The different materials show different trend with similar hysteresis when both Stress and Elongation are normalized (see the insert fig. 4-b). It is worth noting that the work involved (spent) in the cycle is related to the integral under the stress-elongation curve.

The temperature rise for the initial and reversible cycle for the different materials is given in figure 4-c. We note that natural rubber represents the highest temperature rise amongst the tested materials for the reversible cycle. The temperature rise denotes the thermal energy involved during the cycle, under the assumption of adiabatic transformation.

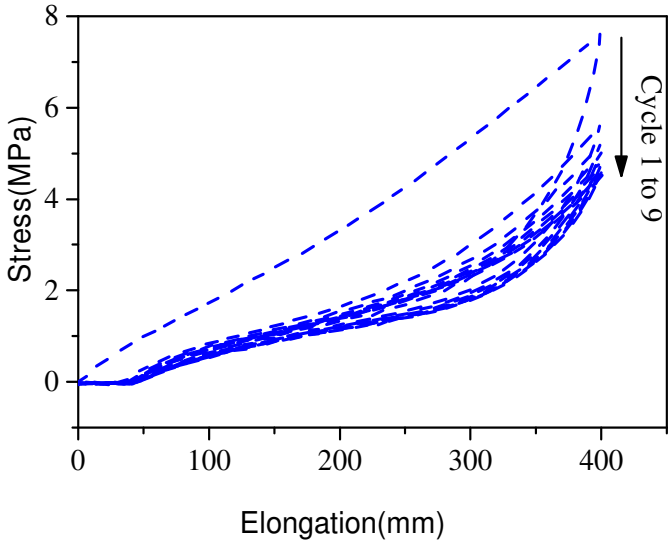

(a)

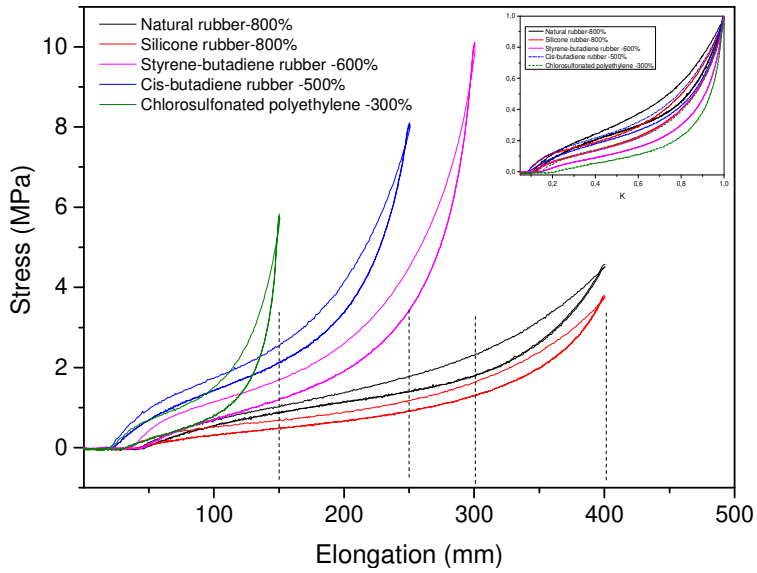

(b)

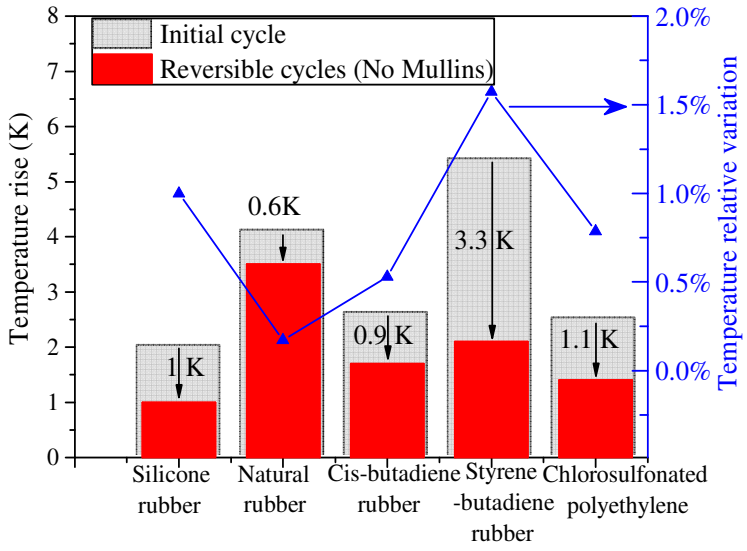

(c)

Fig. 4 Experimental results of Mullins effect elimination. **a.** Reversibility (Mullins effect) of the cycle for natural rubber under 800% strain; **b.** Stress-Elongation curve for different working materials; **c.** Temperature rise for the initial and reversible cycle for the different materials. (sample of 130mm with 50 mm in central part)

4 Analysis of natural rubber refrigeration cycle

4.3 Experimental results and analysis

Figure 5 shows the temperature change of natural rubber surface when the elongation rate is 600 mm.s^{-1} and the strain is 600%. The surface rubber average temperature is measured using Infra-red camera

and we emphasize that the temperature inside the rubber will be higher (or lower) because the inner profile is parabolic, i.e. temperature profile with constant inner positive (negative) source term. As the thickness of the material is 2mm we will consider that this difference is small. From figure 5, we can deduce that an equivalent refrigeration cycle can be divided into four fundamental stages. The first stage is the stretching stage, which duration is dependent on the stretching velocity (elongation rate). In this study, the typical time is 0.5 s. The second stage is the cooling stage via direct contact or/and forced convection (natural convection in our experiments). The third stage includes the release of the sample to go back to its original length. This stage induces a further decrease of temperature. The temperature of the rubber will then increase in a fourth stage to the ambient one.

The dependence of heat rate and ΔT on loading/unloading can be explained by the different kinetics of strain-induced crystallization and crystallite melting, e.g. [34-35].

In order to achieve an equivalent practical refrigeration cycle, the rubber needs to be cooled to the ambient temperature by means of forced convection to minimize the time cycle. In this experiment, the cooling occurs essentially by natural convection, so the time needed to cool the rubber is longer, ~100 s. Comparing the cooling time and the heating time, it is obvious that the heating time is longer than the cooling time, this will be discussed later. It can also be seen from figure 5 that the temperature amplitude of rubber changes little during a cycle.

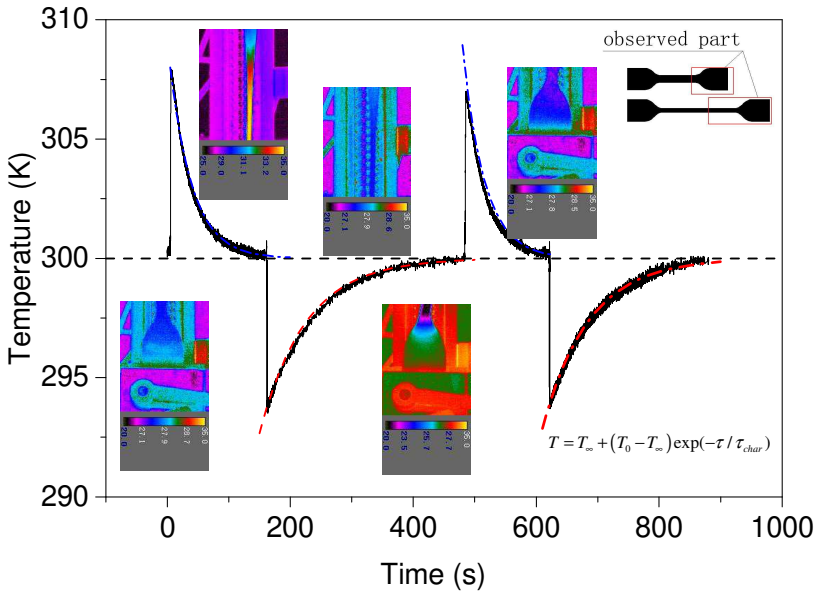

Fig. 5 Development of the temperature curve in two consecutive cycles.
The inserts illustrate the IR image used to extract the observed temperature

From figure 5 it can be noticed that there is an obvious temperature gradient on the observed part of

the rubber at the end of the stretching stage and the end of the recovery stage (see thermographic insets). During the stretch or recovery stage, the fixed part of the rubber is slightly affected by the tension which induces small temperature change.

The analysis of the obtained results on the consecutive cycles shows clearly that the characteristic time of temperature dampening is faster during a stretching phase (36s) than during releasing phase (75s). We therefore obtain a time ratio of release/stretch of 2.1. This question will be analysed theoretically in what follows. The natural rubber temperature increases due to the heating source, *Src*, induced by the stretching for a given maximum elongation (*Elong*.) and elongation rate (Speed). This is given, at a given time, by;

$$\rho c_p V \frac{d\theta}{d\tau} = Src(Elong.,\ Speed) \tag{2}$$

so the temperature increase is given by $\Delta\theta = \frac{\int_0^t Src(Elong., Speed)\, d\tau}{\rho c V} = \frac{E(Elong., Speed)}{\rho c V}$

where E is the energy generated by the material for the imposed elongation (Elong.) and stretching speed (elongation rate). The heating/cooling source term induced by the material deformation and under the assumption of relative constant density we can adopt a constant volume V. During the heating/cooling stage, because the thickness of the rubber (~ 2mm) the energy balance can be written as:

$$\rho c V \frac{d\theta}{d\tau} = -h\ A\ \theta \tag{3}$$

Where $\theta = T - T_\infty$ and the initial condition is $\theta(0) = T_0 - T_\infty = \theta_0$.

Equation (3) can be solved, yielding

$$\frac{\theta}{\theta_0} = \frac{T - T_\infty}{T_0 - T_\infty} = \exp(-\frac{hA}{\rho c V}\tau) \tag{4}$$

The change in temperature follows

$$\frac{T - T_\infty}{T_0 - T_\infty} = \exp(-\tau / \tau_{cr})$$
$$\tau_{cr} = \frac{\rho c}{h}\frac{V}{A} = \frac{\rho c}{h}\frac{Sur}{L_p} \tag{5}$$

where *Sur* and L_p are the elastomer transversal section and perimeter, respectively. A is the external surface of the sample which is the area of heat transfer (m^2). V is the volume for heat storage (storing heat capacity) (m^3), ρ and *c* are the density($kg.m^{-3}$) and specific heat capacity J $(kg \cdot K)^{-1}$, respectively.,

h is the natural convection coefficient (W $m^{-2} \cdot K^{-1}$).

The ratio of characteristic times for two consecutive step, stretching and release is given by;

$$\tau_{cr\_strech} / \tau_{cr\_release} = \frac{L_{p0}}{L_p} \frac{Sur}{Sur_0} \tag{6}$$

We must emphasize that the heat transfer area between clamps and the tested polymer is smaller than that between polymer and ambient so the longitudinal conduction is negligible. However, this ratio is different between the two extrema length situation and can contribute in the case of thicker rubber to the non-symmetrical behavior. Equation 6 can be rewritten using the thermal conductivity of the rubber in order to express the representative time versus thermal diffusivity and Biot number as,

$$\tau_{cr} = \frac{\rho c / \lambda}{h / \lambda} \frac{Sur}{L_p} = \frac{\rho c}{\lambda} \frac{\lambda}{h\left(Sur / L_p\right)} = \frac{\alpha}{Bi} \tag{7}$$

In case of a cylindrical geometry, equation (6) can be simplified as;

$$\tau_{cr\_strech} / \tau_{cr\_release} = \left(Elong.\right)^{-1/2} \tag{8}$$

Figure 6 shows the temperature change for different elongations of the natural rubber. Figure 6 (a) shows the temperature evolution of the sample in time for various elongations and a theoretical fit which uses equation (5) to extract the temperature difference. This difference is deduced from the extrapolation of the fit around τ equating zero and adopting an adiabatic hypothesis. It can be noticed that the temperature decrease in the release stage is lower than the temperature increases in the stretching stage. It is also found that the temperature difference will increase with the increase of the strain, and the cooling time and the heating time also increase. For the different elongation we found that the relaxation time is smaller for the stretching cycle than the one for the releasing cycle.

Temperature differences are plotted in Figure 6 (b) showing both the experimental and fitted data. The cooling characteristic time is extracted and shown in Figure 6 (c) for the investigated elongations. It can be noted that the cooling characteristic time decreases with the growth in the sample elongation. It is important to stress that the stretching of the material tends to increase the length and decrease the cross-section area of the sample. This agrees with equation (6) relating the geometry of the sample *i.e.* perimeter and cross section. The observed tendency and the simplified analytical approach will be helpful during material characterization and design optimization.

The analytical expression for the characteristic damping time obtained from the model *i.e.* eq. (8) is

plotted in figure 6 (c) together with the experimental data for natural rubber. The agreement between the analytical expression and experimental data is reasonable and reflects the observed trends. The right-hand side of figure 6 (c) shows the ratio between the two characteristic times for stretching and release as a function of elongation. The ratio of these two times is found to decrease with elongation and follows the trend described analytically by equation (8).

Figure 7(a) shows the temperature change of 400% strain at different stretch speeds for natural rubber. Some observations can be made as follows; first the temperature change has a weak dependence on the elongation rate, which agrees with the results in [22]. The second is that the time of the cooling stage or the time of the heating stage increases with the decrease of the elongation rate.

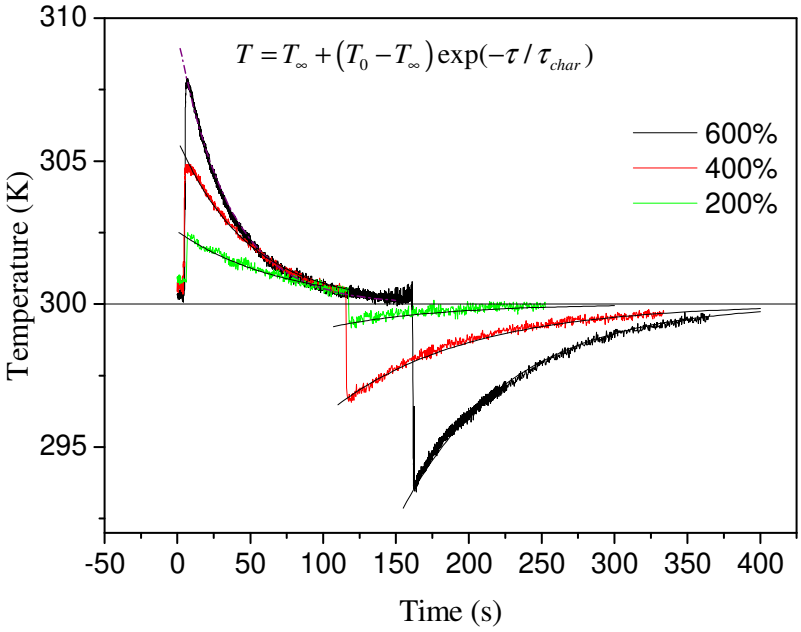

(a)

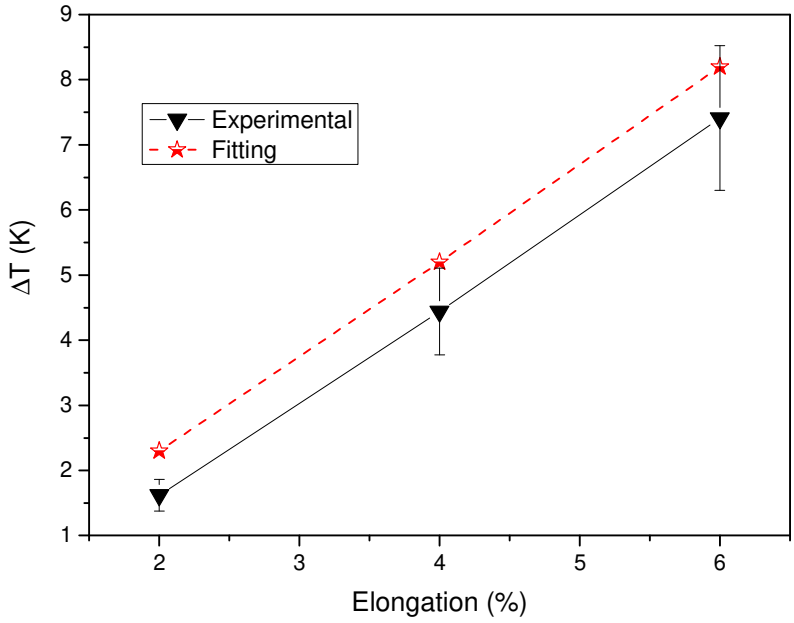

(b)

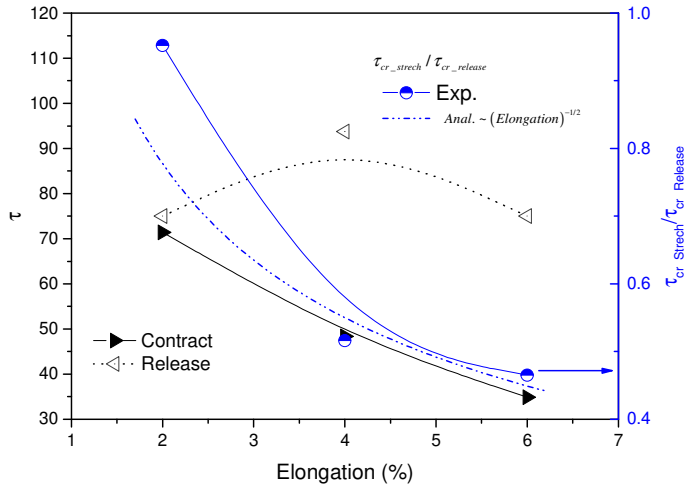

(c)

Fig. 6 (a) temperature evolution in time for various elongations. (b) temperature difference curves *v.s.* elongation. (c) characteristic time as a function of elongation under a stretch velocity of 600mm.s^{-1}.

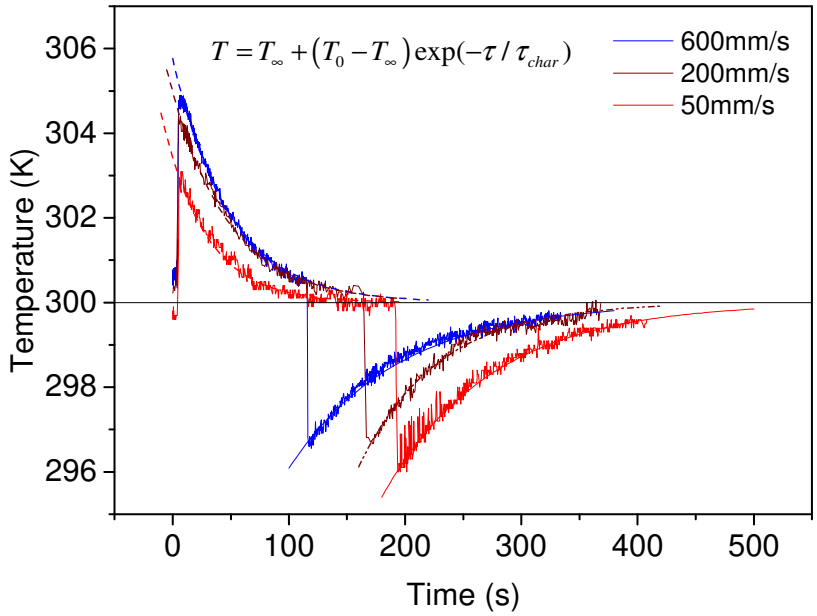

(a)

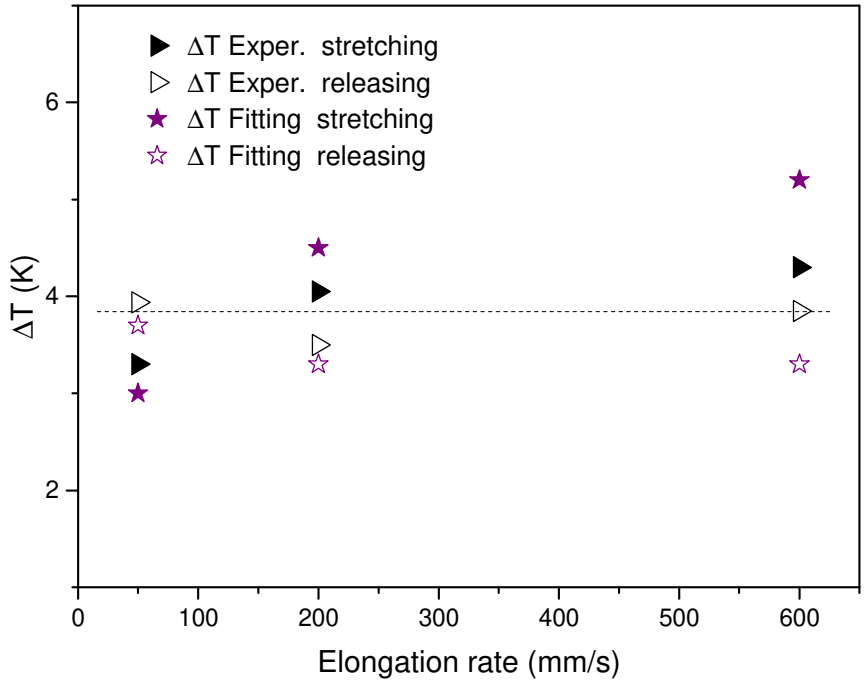

(b)

Fig.7 (a)Temperature curves with different stretch velocity under a strain of 400%. (b) Temperature difference extracted from Figure 7 (a), as a function of elongation rate comparing experimental data and fits.

The temperature difference, extracted from figure 7(a) is plotted in figure 7(b) as a function of the elongation rate. The temperature difference shows little dependence on elongation rate in comparison with the linear dependence we found with elongation (Fig. 6). The comparison of the experimental data

with the fitting data shows a satisfactory agreement. Previous work [37] indicated that strain-induced crystallization varies with stretch velocities which can explain the behavior and part of the observed scatter in our results.

In order to assess the performance of the selected working materials, a Coefficient Of Performance (COP) is introduced. This is the ratio between the extracted thermal energy Q_c obtained during release (cooling) and the provided mechanical work W, see Figure 3. Work (per unit transversal area and per length) is calculated from Figure 4 which represents stress as a function of displacement. The integral in Figure 4 represents this work W. The results for the various working materials are summarized in Table 2. This gives the thermal energy, the work and the corresponding COP. The results for the COP clearly show natural rubber having the best performance compared to all other tested materials.
The given COP is determined by the ratio of thermal energy and input work, which only characterizes the investigated conditions (used protocol, Fig. 3). During refrigeration, the required hot and cold temperature reservoirs as well as the mechanism to transfer heat between the reservoirs will modify the performance. The mentioned and discussed efficiency within our protocol is to compare the different materials. This would be qualitative indication as the real efficiency has to be analysed rigorously through comparison of the obtained COP to the Carnot one [36].

Table 2: Coefficient of Performance (COP) for the selected working materials

Working Material	ΔT	Energy= (ρ.Cp.ΔT) [kJ. m^{-3}] (See Table 1)	Work for stretching= $\int S_T \times d(x/L_0)$ [kJ.m^{-3}]	$COP = {Q_c}/{W}$	Entropy $S = {Q_c}/{T_{ambient}}$ [kJ.(Km^3)$^{-1}$]
Natural rubber	3.5	5219	2.51×103	2.083	17.51
Silicone rubber	1	1497	1.09×104	0.137	5.02
Cis-butadiene rubber	1.7	2547	1.12×104	0.226	8.55
Styrene-butadiene rubber	2.1	3187	1.06×104	0.30	10.69
Chlorosulfonated polyethylene	1.4	2184	7.36×103	0.296	7.33

S_T being the stress.

To have a better representation of the performance results and for the sake of comparison these are plotted in Figure 8. Natural rubber gives the best performance in the form of more than four times than

the next best. This is due to a relatively low work required during stretching and a higher generated thermal energy.

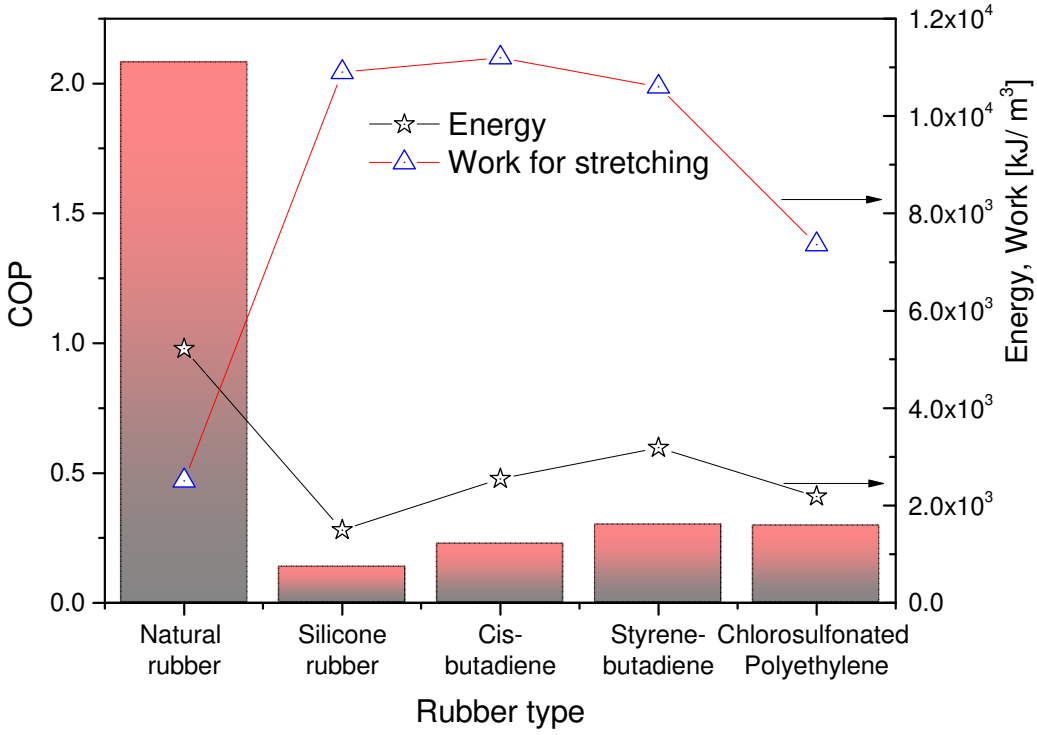

Fig. 8 Comparison of performance results for working materials.

We can conclude that from the pure thermodynamics point of view, natural rubber yields the best performance. Other aspects such as durability as in [8,9] and practicality of the material in real cycles should be given more attention in future studies.

5. Conclusions

Elastocaloric cooling is one alternative which can potentially replace the present mechanical refrigeration systems using refrigerants with environmental detrimental impacts. The objective of the present investigation was to lay the ground for a refrigeration cycle based on elastocalorific effect and calculate in details the Coefficient of Performance (COP) of selected materials. Several (five) rubbers were selected to study their performance. The following conclusions can be drawn:

- The Energy given off thermally increases linearly with the elongation and we have characterized the coefficient that expresses this dependence.
- The Energy is less sensitive to the speed, nonetheless we need to keep a minimum speed to maintain the needed temperature difference, ΔT.
- The cooling (or equivalent heating) behavior to return to the initial state is given by a

characteristic time (damping) dictated by the elastomer geometry and the external conditions (convective heat transfer coefficient). We define a protocol, identify the corresponding values for all the presented tests and we discuss the underlying link between parameters.

- The decrease of the thermal characteristic time with stretching speed, allows better cycle power. The limitation of this improvement was identified and compromise between the speed cycling and the exchange characteristic time.
- After identifying the adequate material and identifying the Energy involved for given elongation (and speed) we have completed our protocol to gain access to the Coefficient Of Performance and the cycle power by choosing the adequate elastomer geometry and the external cooling level.
- Natural rubber is demonstrated to still have the best performance and highest Coefficient Of Performance within the proposed testing protocol.
- The temperature difference of the stretching stage is higher than that of the recovery stage. We discuss ways to avoid such non-symmetrical behaviors.

In the present study, we also find that in order to obtain a more in-depth understanding of the results, there is a need to study the molecular structure of rubber. Nonetheless the present results provide a protocol and basic rules (characterizing the material on simplified protocol, hierarchy on the controlling parameters: elongation, elongation rate, size ..) for the design of a real refrigeration system using natural rubber in normal temperature conditions, such as the cooling process and heating process.

Nomenclature

A	sample external surface
Bi	Biot number
c	specific heat capacity J $(kg \cdot K)^{-1}$, $c_p = e^2 / (\lambda \rho)$
e	thermal effusivity ($Ws^{1/2}m^{-2}K^{-1}$)
E	energy generated by the material under elongation / stretching
L_p	sample perimeter
Q	thermal energy
V	volume for heat storage (heat capacity) (m^3),
$S()$	source/sink term
T	Temperature
W	work
s	entropy
Src	*Energy source term*
Sur	elastomer transversal section transferring (m^2).
h	natural convection coefficient ($W\ m^{-2} \cdot K^{-1}$).

Greek

α	thermal diffusivity
λ	thermal conductivity $[W(m \cdot K)^{-1}]$
$\theta = T - T_\infty$	temperature difference in relative to ambient one
ρ	density ($kg.m^{-3}$)
σ	stress [Pas]
τ	characteristic time

Subscript

Ambient	ambient condition
cr	characteristic
c	cold
h	hot

Acronyms

COP	Coefficient Of Performance

1 *Elong*. Elongation

References:

[1] C.J. William Goetzler, Robert Zogg, Jim Young, (2014) Energy Savings Potential and RD & D Opportunities for Non- Vapor-Compression HVAC, Navig. Consult. Inc., Prep. US Dep. Energy..

[2] Takeuchi, I., & Sandeman, K. (2015). Solid-state cooling with caloric materials. Physics Today, 68(12), 48–54. doi:10.1063/pt.3.3022.

[3] Mañosa, L., Planes, A., & Acet, M. (2013). Advanced materials for solid-state refrigeration. Journal of Materials Chemistry A, 1(16), 4925. doi:10.1039/c3ta01289a.

[4] Brück, E. (2005). Developments in magnetocaloric refrigeration. Journal of Physics D: Applied Physics, 38(23), R381–R391. doi:10.1088/0022-3727/38/23/r01.

[5] Greco, A., Aprea, C., Maiorino, A., & Masselli, C. (2019). A review of the state of the art of solid-state caloric cooling processes at room temperature before 2019. International Journal of Refrigeration. doi:10.1016/j.ijrefrig.2019.06.034.

[6] Tušek, J., Engelbrecht, K., Millán-Solsona, R., Mañosa, L., Vives, E., Mikkelsen, L. P., & Pryds, N. (2015). The Elastocaloric Effect: A Way to Cool Efficiently. Advanced Energy Materials, 5(13), 1500361. doi:10.1002/aenm.201500361.

[7] Chauhan, A., Patel, S., Vaish, R., & Bowen, C. R. (2015). A review and analysis of the elasto-caloric effect for solid-state refrigeration devices: Challenges and opportunities. MRS Energy & Sustainability, 2. doi:10.1557/mre.2015.17.

[8] Uchil, J., Mahesh, K. ., & Ganesh Kumara, K. (2001). Calorimetric study of the effect of linear strain on the shape memory properties of Nitinol. Physica B: Condensed Matter, 305(1), 1–9. doi:10.1016/s0921-4526(01)00593-2.

[9] Kim, K., & Daly, S. (2013). The effect of texture on stress-induced martensite formation in nickel–titanium. Smart Materials and Structures, 22(7), 075012. doi:10.1088/0964-1726/22/7/075012.

[10] Chluba, C., Ge, W., Lima de Miranda, R., Strobel, J., Kienle, L., Quandt, E., & Wuttig, M. (2015). Ultralow-fatigue shape memory alloy films. Science, 348(6238), 1004–1007. doi:10.1126/science.1261164.

[11] Bechtold, C., Chluba, C., Lima de Miranda, R., & Quandt, E. (2012). High cyclic stability of the elastocaloric effect in sputtered TiNiCu shape memory films. Applied Physics Letters, 101(9), 091903. doi:10.1063/1.4748307.

[12] Cui, J., Chu, Y. S., Famodu, O. O., Furuya, Y., Hattrick-Simpers, J., James, R. D., … Takeuchi, I. (2006). Combinatorial search of thermoelastic shape-memory alloys with extremely small hysteresis width. Nature Materials, 5(4), 286–290. doi:10.1038/nmat1593.

[13] Zhang, Z., James, R. D., & Müller, S. (2009). Energy barriers and hysteresis in martensitic phase transformations. Acta Materialia, 57(15), 4332–4352. doi:10.1016/j.actamat.2009.05.034.

[14] Bonnot, E., Romero, R., Mañosa, L., Vives, E., & Planes, A. (2008). Elastocaloric Effect Associated with the Martensitic Transition in Shape-Memory Alloys. Physical Review Letters, 100(12). doi:10.1103/physrevlett.100.125901.

[15] Qian, S., Geng, Y., Wang, Y., Ling, J., Hwang, Y., Radermacher, R., … Cui, J. (2016). A review of elastocaloric cooling: Materials, cycles and system integrations. International Journal of Refrigeration, 64, 1–19. doi:10.1016/j.ijrefrig.2015.12.001.

[16] Maki T. Ferrous shape memory alloys[M]. Cambridge,UK:Cambridge University Press,1988.

[17] Li, S., Cong, D., Sun, X., Zhang, Y., Chen, Z., Nie, Z., … Wang, Y. (2019). Wide-temperature-range perfect superelasticity and giant elastocaloric effect in a high entropy alloy. Materials Research Letters, 7(12), 482–489. doi:10.1080/21663831.2019.1659436.

[18] Yoshida, Y., Yuse, K., Guyomar, D., Capsal, J.-F., & Sebald, G. (2016). Elastocaloric effect in poly(vinylidene fluoride-trifluoroethylene-chlorotrifluoroethylene) terpolymer. Applied Physics Letters, 108(24), 242904. doi:10.1063/1.4953770.

[19] Xie, Z., Sebald, G., & Guyomar, D. (2017). Comparison of elastocaloric effect of natural rubber with other caloric effects on different-scale cooling application cases. Applied Thermal Engineering, 111, 914–926. doi:10.1016/j.applthermaleng.2016.09.164

[20] Joule, J. P. (1859). On Some Thermo-Dynamic Properties of Solids. Philosophical Transactions of the Royal Society of London, 149(0), 91–131. doi:10.1098/rstl.1859.0005.

[21] Dart, S. L., Anthony, R. L., & Guth, E. (1943). Rise of Temperature on Fast Stretching of Synthetics and Natural Rubbers. Rubber Chemistry and Technology, 16(1), 178–183. doi:10.5254/1.3540096.

[22] Guyomar, D., Li, Y., Sebald, G., Cottinet, P.-J., Ducharne, B., & Capsal, J.-F. (2013). Elastocaloric modeling of natural rubber. Applied Thermal Engineering, 57(1-2), 33–38. doi:10.1016/j.applthermaleng.2013.03.032.

[23] Xie, Z., Sebald, G., & Guyomar, D. (2015). Elastocaloric effect dependence on pre-elongation in natural rubber. Applied Physics Letters, 107(8), 081905. doi:10.1063/1.4929395.

[24] Xie, Z., Sebald, G., & Guyomar, D. (2016). Comparison of direct and indirect measurement of the elastocaloric effect in natural rubber. Applied Physics Letters, 108(4), 041901. doi:10.1063/1.4940378.

[25] Wiegand W B. Tendencies in Rubber Compounding[J]. Institution of the Rubber Industry: Transactions and Proceedings,1925,1:141-70.

[26] Hayward,Roger. quoted in Stong C L. (1956). The amateur scientist: mostly about the collection and study of fossilized seeds[J]. Scientific American, ,194:149-158.

[27] Gerlach D W, Alvarado J L, Mina E M,et al. Analysis of elastomer refrigeration cycles[C].

International Refrigeration and Air Conditioning Conference,2002,Paper 538.
[28] Xie, Z., Sebald, G., & Guyomar, D. (2017). Temperature dependence of the elastocaloric effect in natural rubber. Physics Letters A, 381(25-26), 2112–2116. doi:10.1016/j.physleta.2017.02.014.
[29] R. Wang, S. Fang, Y. Xiao, et al, Torsional refrigeration by twisted, coiled, and supercoiled fibers, Science 366 (2019) 216–221. doi: 10.1126/science.aax6182.
[30] Aprea, C., Greco, A., Maiorino, A. , Masselli, C., (2018). Solid-state refrigeration: A comparison of the energy performances of caloric materials operating in an active caloric regenerator. Energy, 165, 439-455. 10.1016/j.energy.2018.09.114
[31] C. Aprea, A. Greco , A. Maiorino , C. Masselli (2020). The employment of caloric-effect materials for solid-state heat pumping, International Journal of Refrigeration 109 1–11. doi.org/10.1016/j.ijrefrig.2019.09.011
[32] Wang Lan, Wang Peizhang, Lu Xiaozhong, Polymer Materials[M]. China Light Industry Press,2009.
[33] Müller, S., Kästner, M., Brummund, J., & Ulbricht, V. (2011). A nonlinear fractional viscoelastic material model for polymers. Computational Materials Science, 50(10), 2938–2949. doi:10.1016/j.commatsci.2011.05.011.
[34] Le Cam J.B., (2017) Energy storage due to strain-induced crystallization in natural rubber: the physical origin of the mechanical hysteresis. Polymer; 127: 166-173;
[35] Plagge, J. and M. Klüppel, A Theory Relating Crystal Size, Mechanical Response, and Degree of Crystallization in Strained Natural Rubber, Macromolecules 2018, 51, 3711-372
[36] Qian S., Nasuta D., Rhoads A., Wang Y., Geng Y., Hwang Y., Radermacher R., Takeuchi I. (2016), Not-in-kind cooling technologies: A quantitative comparison of refrigerants and system performance, International Journal of Refrigeration, , 62, Pages 177-192
[37] Candau, N., Chazeau, L., Chenal, J.-M., Gauthier, C. & Munch, E. (2015). Compared abilities of filled and unfilled natural rubbers to crystallize in a large strain rate domain. Compos. Sci. Technol. 108, 9-15, doi.org/10.1016/j.compscitech.2014.12.014